Available online at www.sciencedirect.com

ScienceDirect

Procedia Chemistry 1 (2009) 425–428

Procedia Chemistry

www.elsevier.com/locate/procedia

Proceedings of the Eurosensors XXIII conference

NEMS/CMOS sensor for monitoring deposition rates in stencil lithography

Marc Sansa[a], Julien Arcamone[a], Jaume Verd[b], Arantxa Uranga[b], Gabriel Abadal[b], Núria Barniol[b], Veronica Savu[c], Marc A. F. van den Boogaart[c], Juergen Brugger[c], and Francesc Perez-Murano[a,*]

[a] *CNM-IMB, Campus UAB, 08193 Bellaterra (Barcelona), Spain*
[b] *Department of Electronic Engineering, ETSE-UAB, Campus UAB, 08193 Bellaterra (Barcelona), Spain*
[c] *Microsystems Laboratory (LMIS1), EPFL, CH-1015 Lausanne, Switzerland*

Abstract

A nanoelectromechanical mass sensor is used to characterize material deposition rates in stencil lithography. The material flux through micron size apertures is mapped with high spatial (below 1 µm) and deposition rate (below 10 pm/s) resolutions by displacing the stencil apertures over the sensor. The sensor is based on a resonating metallic beam (with submicron size width and thickness) monolithically integrated with a CMOS circuit, resulting in a CMOS/NEMS self-oscillator. The sensor is used to test alignment for multi-level nanostencil lithography.

Keywords: Nanomechanical mass sensors; CMOS sensors; nanostencil lithography, nanolithography;

1. Introduction

Shadow masking (also known as nanostencil lithography, SL) is a well known technique to fabricate patterns on a surface [1]. It is a versatile method that can be used in a variety of applications. There has been recently a strong interest regarding the use of shadow masks, mostly related to combinatorial materials science, organic based device fabrication, as well as rapid prototyping of nanoscale structures, using dynamic or quasi-dynamic stencil deposition. [2-9] Its main features are its 'cleanliness', its flexibility, its parallelism and its high resolution. This exclusive characteristic makes that ultra-clean surfaces can be obtained with high purity deposits. Its parallelism allows to improve the throughput of nanoscale patterning in comparison with techniques like FIB or EBL. Recently it has been demonstrated its implementation at full-wafer scale with 150 nm resolution. [10]

* Corresponding author. Tel.: (+34) 93 594 77 00 (ext 2113); fax: (+34) 93 580 14 96.
E-mail address: francesc.perez@imb-cnm.csic.es.

1876-6196/09/$– See front matter
doi:10.1016/j.proche.2009.07.106

Having alignment capabilities, in combination with a large range and highly accurate XY nanopositioning stage, enables to perform stencil lithography in a quasi-dynamic approach [11]. This technique allows multiple nanometer scale patterns of multiple materials, as well as the opportunity to form high purity deposits, as the vacuum is not broken in between each nanopatterning step. The use of a dedicated mass sensor with spatial resolution allows performing the alignment detection using the flux of atoms through small apertures in the stencil membrane, i.e., sharing the same elements already existing in stencil lithography systems.

2. Experimental Set-up

Figure 1.a schematically describes the overall system. The substrate and the sensor are clamped to the same holder, which is fixed to the metal evaporation chamber. The most optimal situation is to have the sensor co-planar with the sample, but, because of packaging limitations in the present configuration, it is located behind the substrate, which has additional apertures to allow the material flux to reach the sensor. The stencil is located below the substrate and parallel to it. The stencil has apertures which are employed to realize the patterns as well as dedicated alignment apertures. The mass sensor detects when these alignment apertures are exactly on top of it, and so, a reference position can be set. The stencil holder is linked to a highly accurate nanopositioning XYZ stage, providing motion of the stencil relative to the rest of the system. The entire system is computer controlled, using software developed in-house.

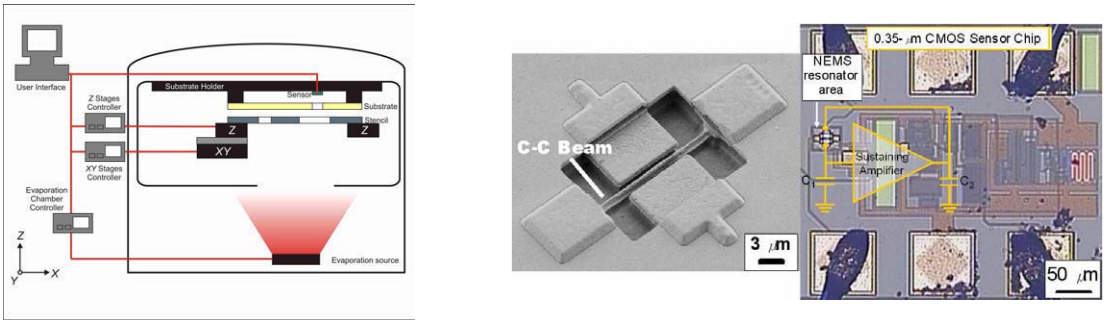

Fig 1. (a) Diagram showing the overall stencil system with sensor alignment. (b) SEM image of the nanomechanical resonator (left) and optical image showing the sensor + CMOS circuit

3. Nanomechanical mass sensor

The electromechanical mass sensor structure is a 18 μm long, 600 nm wide, 850 nm thick (nominal dimensions) resonant doubly clamped beam, whose metallic structure is fabricated with the top metal layer of a commercial 0.35 μm CMOS technology (see Fig. 1.b).

Two lateral electrodes, placed at 600 nm from the resonator on both sides, are used for electrostatic actuation and capacitive readout. The electromechanical resonator is monolithically integrated with a CMOS oscillator circuit. The resonance frequency of the CMOS-NEMS is around 14 MHz, with a quality factor around 1000 in vacuum. The mass sensitivity of this device has been calibrated by depositing a 2 nm thick silver layer, indicating an areal mass sensitivity of 3.4×10^{-11} g.cm^{-2}.Hz^{-1}. The resonator is electrostatically self-excited so that it sets the oscillation frequency of the entire oscillator circuit [12]. The frequency stability level (measured in terms of Allan deviation), combined with the device mass sensitivity, leads to a mass resolution of δM = 450 pg.cm^{-2}, corresponding to a thickness resolution of 0.43 pm for Ag deposition. As a result, the NEMS sensor structure used here presents the following specific features: (i) a high mass resolution which allows detecting deposition rates below 10 pm·s^{-1} for Ag deposition, better than state-of-the-art quartz crystal microbalances QCM; (ii) its small size intrinsically provides

a spatial resolution in the range of hundreds of nm which allows a position-dependent detection; (iii) device portability, because the sensor actuation and readout are completely electrical (CMOS integration).

4. Modeling

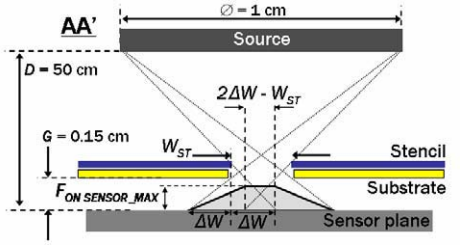

Fig 2. Pattern widening effect as a function of the geometrical dimensions of the system, for $W_{ST} < 2\,\Delta W$.

The alignment accuracy is related with the dimensions of the alignment apertures in the stencil and the dimensions of the sensor: the smaller they are, the most accurate will the position sensing be. When decreasing those dimensions, less signal (material) is arriving to the sensor, so that high sensitivity (mass) sensors are required. In the following, we model the spatial distribution of the deposition rate below the stencil as a function of the overall system dimensions [13].

In shadow masking, a purely geometrical dispersive effect leads to pattern widening when the vertical distance between stencil apertures and substrate, defined as the gap *G*, is not null. The resulting pattern is inherently wider than the nominal one which is defined by the aperture dimensions. The pattern widening ΔW on each side is given by:

$$\Delta W = \frac{1}{2}\frac{SG}{D} \approx 15\,\mu m \tag{1}$$

where *S* is the source diameter (~ 1 cm) and *D* is the source-sensor vertical distance (~ 50 cm). In our system, the gap *G* is 1.5 mm, constrained by the sensor packaging. This limitation has two consequences: the positioning accuracy is potentially decreased, and the specifications on the sensor performance are more restricting due to the fact that a smaller material flux is received per unit area on the sensor plane, i.e. the sensor needs to be more sensitive.

Considering an aperture between substrate and stencil with lateral dimension W_{ST}, when $W_{ST} < 2\,\Delta W$ (see Fig. 2), and more generally when small apertures are used with large gaps, an important issue arises: the deposition rate on the sensor plane becomes smaller than the nominal source flux because of the "penumbra" effect, which in practice obscures part of the whole source area. Then the area of maximum flux on the sensor plane A_{MAX} is then given by:

$$\left(2\Delta W - W_{ST\_X}\right)\left(2\Delta W - W_{ST\_Y}\right) \tag{2}$$

The material fluxes impacting on the sensor are extremely small and require high-performance mass sensors, with spatial and mass resolutions better than the ones provided by the state-of-the-art quartz crystals microbalances.

5. Experimental results and alignment

Fig. 3.a depicts the change of frequency while scanning the stencil and a hole crosses over the sensor. Its derivative directly corresponds to the instantaneous and spatially resolved deposition rate. Apertures on the stencil are designed as two orthogonal rectangles (slits), for aligning in the *X* and *Y* axes. The stencil also contains another set of apertures which are specifically dedicated to the definition of patterns on the substrate.

To estimate the angular error, an alignment procedure is performed (figure 3.b): it consists in successively displacing the stencil along the *X*-axis but at two different *Y* positions. The variation of the *X* position, ΔX, where the

change of resonance frequency occurs is related to the relative angle between the stencil pattern and the *XY* axis of the stage. Knowing ΔX and ΔY (*Y* step between both *X* scans), the angular error can be determined and further compensated by software.

$$\theta = \arctan\frac{\Delta X}{\Delta Y} \tag{3}$$

The present alignment resolution of this system is estimated as following: we consider the resolution to be the uncertainty in the determination of the mid-point of the transition zone of frequency shift (i.e. wherever $d\Delta f_{RES}/dX \neq 0$). It approximately stands in the range of 1 μm. We can define the angular misalignment resolution as the minimum angle the system can correct. This parameter is limited by the resolution of the system, that is, the minimum ΔX we can detect. Therefore we can estimate the angular misalignment resolution from (3). Using our current system resolution (1μm) and considering an alignment aperture (ΔY) of 400 μm, the angular misalignment resolution is 0.143 degrees. This parameter has been validated experimentally, leading to an angular resolution lower than 0.15 degrees.

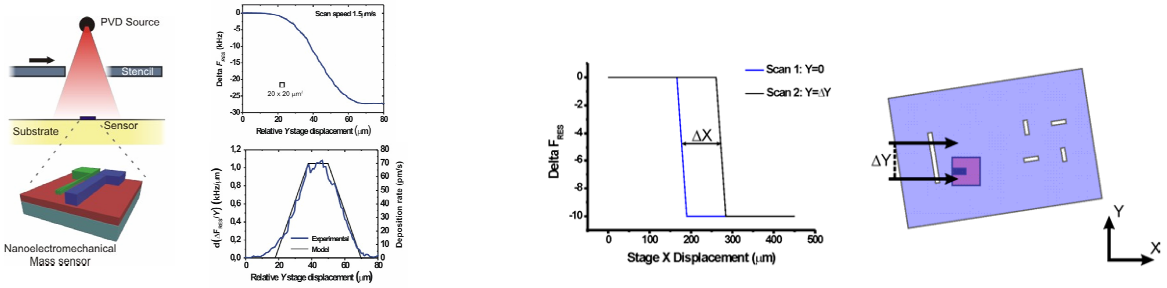

Fig.3. (a) Experimental determination of the evaporation rate of an atom beam after passing through an stencil hole. (b) Alignment process using a Nanomechanical mass sensor.

Acknowledgements

The work is partially funded by projects TEC2006-03698/MIC and TEC2006-13910-C03

References

1. J. Brugger, V. Savu, K. Sidler, M.A.F. van den Boogaart, O. Vazquez Mena, G. Villanueva, E-Nano Newsletter, vol 8, pp 22-28, June 2007
2. A. Ludwig, J. Cao, J. Brugger et al., Journal of Combinatorial Chemistry 6 (1), 50-53 (2004).
3. A. Tixier, Y. Mita, J.P. Gouy, H. Fujita; "A Journal of Micromechanics Microengineering; Vol.10; pp. 157-162; (2000)
4. P. F. Tian, P. E. Burrows, and S. R. Forrest Applied Physics Letters 71 (22), 3197-3199 (1997);
5. Y. X. Zhou and A. T. Johnson, Nano Letters 3 (10), 1371-1374 (2003).
6. S. Egger, A. Ilie, Y. T. Fu et al., Nano Letters 5 (1), 15-20 (2005);
7. L. Gross, R. R. Schlittler, G. Meyer et al., Applied Physics Letters 90 (9) (2007);
8. H. M. Guo, D. Martrou, T. Zambelli et al., Applied Physics Letters 90 (9) (2007).
9. Z. Racz, J. L. He, S. Srinivasan et al. Journal of Vacuum Science & Technology B 22 (1), 74-76 (2004).
10. J. Arcamone, M.A.F. van den Boogaart, F. Serra-Graells,; J. Fraxedas, J. Brugger, F. Pérez-Murano; Nanotechnology, 19, 305302 (2008)
11. V.Savu, M.A. F. van den Boogaart, J.Brugger, J. Arcamone, M. Sansa, and F. Perez-Murano. J.Vac.Sci.Technol.B, 26 2054 (2008)
12. Verd, J. Uranga, A. Abadal, G. Teva, J.L. Torres, F. Lopez, J.L. Perez-Murano, E. Esteve, J. Barniol, N. IEEE Electron Device Letters Vol. 29, Issue: 2, 146-148 (2008)
13. J. Arcamone, M. Sansa, J. Verd, A. Uranga, G. Abadal, N. Barniol, M.A.F. van den Boogaart, J. Brugger, F. Perez-Murano, Small, 5, pp. 176-180 (2009)